Robust senescence evaluation by transcriptome-based hUSI to facilitate characterizing cellular senescence under various conditions

Ting Ni (tingni@fudan.edu.cn)
Collaborative Innovation Center of Genetics and Development, Human Phenome Institute, School of Life Sciences, Fudan University https://orcid.org/0000-0001-7007-1072

Jing Wang (jing_w21@m.fudan.edu.cn)
State Key Laboratory of Genetic Engineering, Collaborative Innovation Center of Genetics and Development, Human Phenome Institute, School of Life Sciences and Huashan Hospital, Fudan University

Weixu Wang (weixu.wang@helmholtz-munich.de)
Institute of Computational Biology, Helmholtz Center Munich, Munich, Germany

Jun Yao (junyao18@fudan.edu.cn)
Department of Data System, 3D Medicines Inc, Shanghai, China

Xiaolan Zhou (22112030049@m.fudan.edu.cn)
State Key Laboratory of Genetic Engineering, Collaborative Innovation Center of Genetics and Development, Human Phenome Institute, School of Life Sciences and Huashan Hospital, Fudan University

Gang Wei (gwei@fudan.edu.cn)
Fudan University

Article

Keywords: Cellular senescence, Quantification, Machine learning, hUSI

DOI: https://doi.org/

Additional Declarations: There is **NO** Competing Interest.

Robust senescence evaluation by transcriptome-based hUSI to facilitate characterizing cellular senescence under various conditions

Jing Wang[1#], Weixu Wang[1, 2#], Jun Yao[1,3 #], Xiaolan Zhou[1], Gang Wei[1*], Ting Ni[1*]

[1]State Key Laboratory of Genetic Engineering, Collaborative Innovation Center of Genetics and Development, Human Phenome Institute, School of Life Sciences and Huashan Hospital, Fudan University, Shanghai, 200438, P.R. China

[2] Institute of Computational Biology, Helmholtz Center Munich, Munich, Germany

[3] Department of Data System, 3D Medicines Inc, Shanghai, China

* Corresponding authors: E-mails: tingni@fudan.edu.cn; gwei@fudan.edu.cn;

Contributing authors: jing_w21@m.fudan.edu.cn; weixu.wang@helmholtz-munich.de; junyao18@fudan.edu.cn;

[#] These authors contributed equally to this work.

Abstract

Despite the manifestation and contribution of cellular senescence to tissue aging and aging-related disease, the identification of *in vivo* senescent cells and the recognition of senescence-specific communication still remain challenging. Current senescence evaluation methods rely greatly on expression level of well-known senescence markers, enrichment of aging-related gene sets or weighted sum of curated genes. However, focusing on limited senescence aspects, these methods could not adequately capture the comprehensive senescence features. To evaluate senescence in a more general and unbiased way from the most common and easily accessible transcriptome data, we developed human universal senescence index (hUSI) to quantify human cellular senescence based on a series of weighted genes learned from representative senescence RNA-seq profiles using a machine learning algorithm. hUSI demonstrated its superior performance in distinguishing senescent samples under various conditions and robustness in handling batch effects and sparse profiles. hUSI could uncover the accumulation of senescent cells of various cell types in complex pathological conditions, and reflected the increasing senescence burden of patients and provided potential senotherapeutic targets. Furthermore, combined with gaussian mixture model, hUSI successfully inferred senescent tumor cells in melanoma and identified key target signaling pathways that are beneficial for patient prognosis. Overall, hUSI provides a valuable choice to improve our ability in characterizing cellular senescence under various conditions, illustrating promising implications in aging studies and clinical situations.

Keywords: Cellular senescence, Quantification, Machine learning, hUSI

1 Introduction

Cellular senescence (CS) characterized by irreversible cell cycle arrest is considered a critical factor for aging and aging-related diseases[1]. For instance, by presenting senescence-associated secretory phenotypes (SASP) including increased secretion of pro-inflammatory proteins and other paracrine factors (such as TGF-β family ligands, VEGF, CCL2 and CCL20)[2], senescent cells can stimulate immune response and cell-cell communication leading pleiotropic effects in various tissues[3]. Targeted clearance of accumulated senescent cells using senolytic drugs[4] or inducing tumor cells into senescence[5] have shown benefits for disease prognosis and healthy lifespan. However, despite several morphological (such as flattening and enlarging[6]) and molecular markers (such as p16[7], p21[8], p15[9] and p27[9]) are used to characterize senescent cells, identification of *in vivo* senescent cells still pose a great challenge due to its heterogeneity[10]. Depending on the real situations, CS in diverse cell types can be induced by various intrinsic and extrinsic stressors, such as replicative stress, oncogene activation, chemotherapeutic drugs and ionizing radiation[11]. Therefore, to properly quantify CS degree in multiple scenarios, there is an urgent need for a universal method which enables sensitive capture of comprehensive senescence features, especially in the era where single-cell transcriptome technology has been widely applied to construct cell atlas of human multiple tissues[12, 13].

Quantifying senescence degree by senescence score is regarded as a convenient and efficient way to monitor senescence status and disease progression[14]. Considering there is no one-size-fits-all marker gene to exclusively indicate senescence, most attempts to evaluate senescent samples mainly depend on the expression level of aging or senescence associated genes derived from differential analysis and literature studies, giving rise to several aging or senescence-associated gene sets (such as CellAge[15] and SenMayo[16]) and senescence scoring methods (such as DAS+MSS[14], CS score[17] and lassoCS[18]). However, due to the variation in gene composition and the limited study dataset (only focus on particular sample type or senescence type), these methods cannot reliably evaluate transcriptional signatures of senescent samples in various contexts and are susceptible to the absence of some pre-defined senescence-related genes. For example, only involving replicative senescence associated genes as the basis for scoring senescence status might produces bias in evaluating senescence in real aging tissues or induced senescence samples. Thus, we sought to utilize publicly available high-quality transcriptome profiles of senescent samples to learn the comprehensive senescence features and develop a reliable and universal senescence score for senescence evaluation.

In the present study, to evaluate cellular senescence in a more general and unbiased way, we introduce hUSI that can accurately assess the burden of senescence at both bulk and single-cell levels. It started from collecting representative senescence transcriptome profiles encompassing multiple contexts, including those derived from different platforms, cell types, conditions, and senescence-induction factors. With the criteria of confirmed senescence status and involving diverse cell and senescence types, we finally collected bulk RNA-seq profiles from five cell types and six senescence types induced by both intrinsic and extrinsic stressors. Then, hUSI was developed based on features extracted from these representative senescence transcriptomes by a machine learning model. hUSI demonstrated high accuracy in distinguishing senescent samples from non-senescent samples in different context. Furthermore, hUSI outperformed other current methods in evaluating senescence at single-

cell level and remained robust and reliable in multiple senescence samples. Intriguingly, hUSI can uncover senescent cell subpopulation, as illustrated in melanoma, that correlated with improved patient survival, indicating its promising potential in clinical situations. Notably, hUSI distinguished typical signaling pathways (such as TGF-β and BMP pathways) that could promote senescence-associated cell-cell communication in tumor microenvironment. Overall, hUSI provides a universal and robust way to measure senescence burden, enabling more comprehensive investigations into senescence in various experimental and clinical context.

2 Results

Development and validation of hUSI

To systematically learn and evaluate the comprehensive signature of CS, we developed a workflow including data collection, data re-processing, feature extraction and quantification of senescence degree (Fig. 1a). We first collected RNA-seq data sets derived from representative human senescence types serving as senescence training samples, which encompassed five cell types (fibroblasts, endothelial cells, astrocytes, melanocytes, and keratinocytes) and six senescence types (ionizing radiation-induced senescence (IRIS), replicative senescence (RS), oxidative stress-induced senescence (OSIS), oncogene-induced senescence (OIS), natural senescence (NS) as well as compound-induced senescence (CIS)), along with the corresponding non-senescent samples serving as young controls[19-27] (Extended Data Fig.1a,b and Supplementary table S1). Next, considering these data sets were derived from different experimental methods and sequencing protocols, we re-preprocessed all the raw data with the same pipeline to generate standard and normalized profiles for feature extraction and validation (Extended Data Fig.1b and Methods). After processing, we found that, as expected, *CDKN1A* and *CDKN2B* (encode the well-known senescence marker p21 and p15, respectively) showed significant higher expression level, demonstrating reliability of samples and the overall analysis pipeline (Fig. 1b).

Then, we went on to acquire features of the senescence profiles by machine learning algorithms. Multiple machine learning algorithms have been employed for mining genes associated with individual aging or CS, such as regression, elastic net, and random forests[28-30], facilitating quantification of senescence degree in tumor and normal cells. However, senescence, as a complicated and continuous state, its heterogeneity has not been fully considered in these models[31]. In this study, we selected one-class logistic regression (OCLR) algorithm to learn the features of senescence transcriptome profiles, as it has been demonstrated superior performance on capturing cell heterogeneity[32]. After training, OCLR learned the features of senescence samples in training set, in other words, all genes were respectively assigned with different weights representing their contributions to senescence (Methods). In our learned-senescence features, except for genes upregulated in CS and associated with SASP (such as *APOD*, *EHF* and *SAA2*)[33-35] were assigned with top weights, some genes with high positive or negative weights while their functions in CS were poorly reported (such as *OLAH*, *CADM3* and *HMSD*) (Extended Data Fig.1c). These results suggest that OCLR not only captures the known senescence features but also identifies potential novel senescence-associated genes. To our surprise, classical senescence marker, including *CDKN1A*, *CDKN2B* and *SERPINE1*, are only assigned with slightly positive weights, probably because of relatively low expression levels in samples (Supplementary table S2). To further

examine the biological interpretability of learned-senescence features, gene set enrichment analysis (GSEA)[36] was performed based on the weight of each gene (Methods). We found that multiple senescence associated gene sets were positively enriched, including interferon-gamma response[37], KRAS signaling[38], inflammatory response[39], hypoxia and p53 pathway[40, 41] (Fig. 1c, left panel). On the contrary, the proliferation associated pathways (such as G2M checkpoint[42], E2F targets[43], mitotic spindles[44] and MYC targets[45]) were in the negative enrichment terms (Fig. 1c, right panel). These results supported the reliability of the features learned by OCLR in reflecting senescence.

In terms of quantifying senescence degree, the Spearman correlation coefficient between gene weights and expression values was selected as the metric to quantify senescence degree, defined as human universal senescence index (hUSI) (Methods). To test the stability and reliability of hUSI, we used leave-one-out cross-validation (LOOCV) strategy to calculate average correctly rank probability (CRP) for each iteration, and the resulted CRP reached 0.9 (Extended Data Fig.1b, d and Methods). We next validated whether hUSI can be influenced by batch effects arising from variations in experimental conditions, sequencing platforms, or analysis pipelines. We compiled bulk RNA-seq datasets from seven independent studies, each comprising oncogene-induced senescent IMR90 cells induced by 4-hydroxytamoxifen (4-OHT), along with corresponding control cells[24, 46-49] (Supplementary table S1). We calculated hUSI for each sample and found that all senescent groups have much higher hUSI values (hUSIs) than the non-senescent groups (Fig. 1d). Besides, with a plethora of genes included in the senescence features for calculation, hUSI is technically more robust to profiles with limited or sparse gene signals such as microarray and single-cell RNA-seq (scRNA-seq) data. Therefore, we applied hUSI on six senescence-related microarray datasets and the most of them were derived from cell types which were not included in training set[50-55]. The results showed that hUSIs were consistently higher in all senescent groups compared to non-senescent ones (Extended Data Fig.2a). To test the robustness of hUSI, we generated simulated sparse profiles from these microarray transcriptome profiles by randomly zeroing-out expression signals. We found that even zeroing-out 50% of genes expression signals, hUSIs still represented higher levels in all senescent groups (Extended Data Fig.2b). All these results suggested that hUSI, based on comprehensive senescence features and effective nonparametric rank-based correlation[56], is pretty stable and robust.

hUSI shows reliable performance in quantifying senescence degree

To assess the generalizability of hUSI, we gathered three bulk RNA-seq datasets (including immortal MDAH04 cells and senescent MDAH04 cells induced by different chemical compounds[57], WI-38 cells treated with 4-OHT for different days[58] and proliferative WI-38 cells and senescent WI-38 cells induced by replication[58]), notably the conditions of these samples are not exactly same as samples in the training set (Supplementary table S1). We found that most senescent groups exhibited significant higher hUSIs compared to non-senescent ones even the sample size is limited (Extended Data Fig.2a). Moreover, hUSI also demonstrated its ability to discern aggravated senescence in samples induced by extended 4-OHT exposure time (Fig. 1e, middle panel).

Next, we calculated hUSIs for a large normal samples dataset obtained from the Genotype-Tissue Expression Project (GTEx). We observed that hUSIs progressively and significantly

elevated with increasing age, consisting with the continuous accumulation of senescent cells in aging process[59] (Fig. 2a). To validate the reliability of hUSI in assessing senescence degree, we calculated Spearman correlation coefficient between hUSIs and CS scores, which was a tool based on conducting gene set variation analysis (GSVA) on a curated set of 1,259 genes derived from studies on replicative cell senescence[17]. The results showed overall positive correlations of these two methods (R = 0.7), and across 29/30 tissues (R from 0.28 to 0.85) (Fig. 2b left panel and Fig. 2c upper panel). The same strategy was applied on a large tumor samples dataset from The Cancer Genome Atlas (TCGA) datasets. Despite the heterogeneity in tumor samples, hUSIs still showed overall positive correlations with CS scores (R = 0.52) and across all cancer types (R from 0.12 to 0.94) (Fig. 2b right panel and Fig.2c lower panel). Of note, we discovered that hUSIs demonstrated higher variations in different cancers compared to CS scores, which might indicate that hUSI enables to reveal more intrinsic heterogeneity of senescence across different tumor types (Fig. 2c lower panel).

hUSI has better performance in distinguishing senescence cells

Given the reliable and robust performance of hUSI on scoring bulk samples under various conditions, we next applied hUSI on four scRNA-seq datasets derived from primary senescent cells induced by various stressors (including oncogene[49, 60], radiation[61], and replication[61], as well as secondary senescent cells triggered by paracrine signals[62]) to assess the robustness of hUSI at single-cell level across diverse conditions. The senescence status of these cells had been confirmed in respective studies by examining senescence marker genes and senescence-associated β-galactosidase (SA-β-Gal) staining[49, 60-62] (Supplementary table S1). Non-senescent cells from each dataset were also included for comparative analysis. After quantifying the senescence degree of each cell using hUSI, we observed significantly higher hUSI levels in senescent groups than non-senescent groups across all four datasets, supporting the applicability of hUSI on scRNA-seq data (Fig. 3a). Next, we compared the performance of hUSI with other three groups of senescence qualification strategies (including those based on gene expression level, computed score and enrichment score of single sample GSEA (ssGSEA)) (Methods).

First, we first obtained 12 well-known CS or proliferation associated markers (*GLB1*, *TP53*, *CDKN1A*, *CDKN2A*, *CDKN2B*, *CDK1*, *CDK4*, *CDK6*, *MKI67*, *LMNB1*, *IL1A*, and *RB1*) and separately used their normalized expression values to directly classify cells, as their upregulation or downregulation is widely employed to identify CS status[63-71]. We found that only *CDKN1A* exhibited a higher trend in senescent samples than control samples across all datasets (Extended Data Fig.3a, left panel). To better compare the performance of hUSI and the markers in classifying senescent cells in limited scRNA-seq datasets, we randomly split each dataset into 10 folds and replicated the process three times, and then calculated the ranks of average Area Under Curve (AUC) of all units in each dataset (Supplementary table S3 and Methods). We observed that hUSI exhibited excellent performance compared to all the tested classical markers (Fig. 3b, left panel and Supplementary table S3).

Second, we compared hUSI with five existing senescence score computing methods, including DAS, mSS and their combination (DAS+mSS)[14], lassoCS[18] and CSS[28]. To our surprise, these methods only gave senescent group a higher score level than control group in certain datasets (Extended Data Fig.3a, middle panel). We then applied the same strategy

above to calculate average AUC ranks. hUSI also achieved the highest average AUC rank compared to all computed senescence scores (Fig. 3b, middle panel). Additionally, we observed that DAS+mSS, as expected, outperformed both DAS and mSS individually (Fig. 3b, middle panel). Of note, except for hUSI, all these methods exhibited substantial variations across four datasets (Fig. 3b, middle panel), supporting the more stable performance of hUSI.

Finally, considering aging and senescence-associated gene sets have been commonly used to quantify CS by enrichment score using ssGSEA, in the present study, we collected eight publicly available senescence-associated gene sets (including CellAge[15], GenAge[72], ASIG[73], SASP (downloaded from MSigDB under acessesion ID R-HSA-2559582), AgingAtlas[74], SenUp[75],SenMayo[16], and SigRS[76]) to calculated their ssGSEA scores in four scRNA-seq datasets (Supplementary table S4). The result showed that only SenUp gave higher scores for senescent groups than control groups across four scRNA-seq datasets (Extended Data Fig.3a, right panel). After calculating average AUC ranks, hUSI still exhibited superior performance over all gene sets, with minimal variation observed across the four single-cell datasets (Fig. 3b, right panel). Furthermore, we found that genes from all these gene sets can be found in our features, and genes had been assigned with different weights which enable hUSI to capture a broader spectrum of gene expression signals in the senescence evaluation process (Supplementary table S2,4). These results above combined to suggest that hUSI has relative superiority and stability across different scRNA-seq datasets comparing to other current methods.

hUSI enables to evaluate senescence burden in complex conditions

After validating the outperformance of hUSI in distinguishing senescent cells, we next sought to apply hUSI on single-cell data from real pathological tissues. The accumulation of senescent cells has been reported to increase the susceptibility to COVID-19 patients by contributing to SARS-CoV-2-mediated hyperinflammation and cytokine storm[77, 78]. Consequently, the targeted elimination of these senescent cells has been proposed as a potential treatment strategy for COVID-19[77, 78]. However, the deconvolution of senescent status across various cell types in infected lung tissues and the study of detrimental effects of different senescent cells on patient survival are still lack. Thus, to evaluate the senescence burden of COVID-19 patients, we calculated the hUSIs for a single-nuclei RNA-seq (snRNA-seq) dataset (containing a total of 116,313 nuclei) derived from infected and normal lungs with donor age ranging from 58~84 years old[79] (Fig. 3c and Methods). We found that most cell types (including epithelial cells, endothelial cells, fibroblasts, myeloid, and neuronal cells) from COVID-19 patients exhibited significantly higher hUSI values compared to those from normal donors (Fig. 3d). Intriguingly, a reverse trend was observed in B cells and T cells, suggesting the activation of immune cells following COVID-19 infection[80] (Fig. 3d).

To better discern various senescence status, we applied a gaussian mixture model (GMM) to fit the distribution of hUSIs within all tested cells and successfully classified them into four distinct classes (C1~C4) (Fig. 3e, left panel and Methods). Their senescence degrees were further validated by the higher expression level of classical senescence-associated genes (*CDKN1A*, *IL1A*, *IL6*, *IL8*, *CCL2*, *CXCL10*, *MMP9*, *SERPINE1*, *THBS1* and *TIMP1*) and lower expression level of proliferation markers (*LMNB1*, *MKI67* and *DHFR*), consisting with

the reported elevated cell senescence responses to SARS-Cov-2 infection[81] (Fig. 3e, right panel). We also observed that COVID-19 lung tissue has a higher proportion of the most senescent cell class (denoted as C4) cells compared to normal tissue (Fig. 3f), consistent with the reports suggesting a high accumulation of senescent cells in COVID-19 patients[77, 82]. Besides, patients with faster disease progression showed more accumulation of senescent cells (Fig. 3g). These results all suggested that hUSI successfully revealed survival-detrimental senescent cells accumulated in COVID-19 lung tissue across various cell types ◦

We then examined the difference in the fraction of four cell groups for each cell type between COVID-19 and the normal samples. The results showed there are higher fractions of senescent cells existed in the cell types with a higher risk of exposure to SARS-CoV-2 or hyperinflammatory microenvironment, such as monocyte-derived macrophages, inflamed endothelial cells, pathological fibroblasts and alveolar type 1 progenitor cells (AT1) (Fig. 3h and Extended Data Fig.4a, b)[78, 83-85]. While alveolar type 2 progenitor cells (AT2), which are targeted by SARS-CoV-2 through the angiotensin-converting enzyme 2 (ACE2), was reported to exhibit apparent senescence and a proinflammatory phenotypes[86], AT1 accumulated in a higher proportion in COVID-19 lung tissue than AT2, possibly because AT2 can differentiate into AT1-like cells for alveolar regeneration in COVID-19 patients[87].

To investigate the alterations in senescent cells, we performed differential gene expression analysis between C4 and C2 (which is the second young class (Fig. 3f)). We did not take C1 class as the control due to its very small cell numbers, which usually lead to some bias in differential analysis. Differential genes (DEGs) of AT1 and AT2 were respectively enriched on KEGG and GO databases. The results showed that senescent AT1 and AT2 cells have enriched on pathways associated with antigen process, extracellular matrix and immune cytotoxicity, especially AT1 has enriched on p53 signaling pathway, indicating a higher relevance of these senescent on infection response, cellular communication and cellular senescence (Fig. 3i and Extended Data Fig.4c). In addition, DEGs were also enriched in senescent monocyte-derived macrophages as it showed largest fraction difference in C4, reaching 0.29, and was reported to drive the inflammatory response to SARS-CoV-2 and contribute to cytokine storms in severe COVID-19[88, 89]. The results showed that pathways, including positive regulation of T cell-mediated immunity and leukocyte-mediated cytotoxicity, was enriched in these cells, indicating their crucial roles of senescent cells in macrophage-mediated clearance of infected cells, which may also cause damages to infected tissues by hyperinflammatory[90] (Extended Data Fig.4d). All these results above demonstrated that hUSI enables to recognize senescent cells that abnormally accumulated in pathological tissue and reveal associated mechanisms.

hUSI identifies immune associated senescent tumor cells in melanoma

We then sought to apply it on tumor samples, as CS plays an important role in tumor development and can activate immune responses[91]. Significant progress has been made in immunotherapy of melanoma, especially with the application of immune checkpoint inhibitors, such as PD-1 antibodies and CTLA-4 antibodies, which result in significant durable responses and therapeutic efficacy[92, 93]. However, the mechanisms underlying immunotherapy remain incompletely understood. Several studies have demonstrated the relationship between senescent tumor cells and immune recognition[94-97], thus we sought to

identify senescent tumor cells and investigate whether it could serve as potential targets for immunotherapy in melanoma.

To explore the characteristics of senescent tumor cells in melanoma, we evaluated the senescence degree of tumor cells by applying hUSI on a melanoma scRNA-seq data set[98]. We then used GMM to infer three cell subpopulations which were denoted as *cycling*, *transactional* and *senescent*, based on the significantly increasing hUSI level (Extended Data Fig.5a, b). The senescence degree of these subpopulations was further validated by a microarray-based transcriptome dataset of melanocytes[52]. By overlapping DEGs of melanocytes bulk samples with specific highly expressing genes in our defined cell subpopulations (Methods), we found that genes up-regulated in senescent melanocytes were significantly enriched in *senescent* and *transitional* subpopulations (Fig. 4a and Supplementary table S5). On the contrary, genes up-regulated in growing melanocytes were significantly enriched only in *cycling* subpopulation (Fig. 4a and Supplementary table S5). We also validated the different senescence degree of these three subpopulations by inferring a senescence trajectory of tumor cells. We imputed 38 co-expression modules based on hUSI-related genes and diffusion map was used for dimensionality reduction and visualization. The senescence trajectory was characterized by the transition of tumor cells from *cycling* to *senescent* status (Fig. 4b and Extended Data Fig..5c, d and Methods). Two well-known senescence hallmark genes, *CDKN1A* and *SERPINE1*, showed higher expression level in *senescent* subpopulation than in the other two subpopulations (*cycling* and *transitional*) (Fig. 4c). Moreover, GSEA results of specific highly expressing genes in each subpopulation indicated more frequent immune activities occurred in senescent tumor cells (Fig. 4d and Methods). These results demonstrated that heterogeneity in senescence existed among melanoma tumor cells, and hUSI can reliably distinguish senescent tumor cells.

We next analyzed the impact of senescent tumor cells on melanoma patient survival. We took three tumor cell subpopulations as a reference expression profile and deconvoluted RNA-seq profiles of melanoma cohort from TCGA-SKCM using EpiDISH[99], obtaining the proportion of each subpopulation in each melanoma patient (Methods). Considering the potential relationship between senescent tumor cells and immune response, we also calculated abundances of 22 immune component using CIBERSORT[100]. We found that the proportion of *senescent* subpopulation have a higher positive correlation with the abundance of M1 macrophage cells, CD8 T cells, and activated immune cells (including activated CD5 memory T cells and activated dendritic cells) (Fig. 4e). Survival analysis was then performed based on the inferred proportions of these subpopulations. The result showed that the higher proportion of *senescent* or *transactional* subpopulations in a patient, the more favorable it was for the patient's survival, and the significance of *senescent* is higher than *transactional* (Fig. 4f). In contrast, patients with higher proportion of *cycling* subpopulation have worse prognosis (Fig. 4f and Extended Data Fig.5e). These results suggested that hUSI-aided senescence state evaluation of tumor cells can serve as a promising prognostic biomarker for melanoma patients.

hUSI recognizes special signaling pathways in senescent melanoma cells

In the above analysis, hUSI helps identify senescent tumor cells in melanoma. However, the role of senescent cells in tumor microenvironment is very complex and highly dependent on

the physiological environment[101-103]. Senescent cells can communicate with neighbor cells and influence their behavior through paracrine signaling. Specifically, SASP presented by senescent tumor cells plays important roles in communication with immune system by attracting immune cells (such as T cells and NK cells) and then leading to the clearance of senescent tumor cells[95-97]. Besides, CS associated communication had been speculated to regulate immune surveillance and influence tumorigenesis[104]. Therefore, understanding how senescent cells interact with the microenvironment may provide additional clues for the relationship between senescence and tumorigenesis.

To explore the cross-talk between senescent tumor cells and the microenvironment in melanoma, we investigated the cell-cell communication between these three tumor cell subpopulations (*cycling*, *transactional and senescent*) and their neighboring cells using CellChat[105] (Fig. 5a). The results showed that the communication strength of hUSI-identified *senescent* subpopulation was higher than the other two relatively less senescent tumor cell subpopulations (*cycling* and *transactional*), indicating stronger cell-cell communication between senescent tumor cells and neighboring cells (Fig. 5b and Extended Data Fig.5f). Furthermore, analysis of the global output communication patterns uncovered two different signaling patterns, with pattern 1 corresponding to the *senescent* tumor subpopulation and pattern 6 corresponding to the *cycling* and *transitional* subpopulations (Extended Data Fig.5g). To analyze which pathways were responsible for senescent tumor cells to receive communication signals from tumor microenvironment, we compared communication strength of each involved signaling pathway (Methods). Six pathways (including transforming growth factor β (TGFβ) pathway, leptin (LEP) pathway, chondroitin sulfate proteoglycan 4 (CSPG4) pathway, chemokine signaling pathways (CCL), CD6 pathway and bone morphogenetic protein (BMP) pathway) were found to have input signal strength to *senescent* subpopulation and not detected in *cycling* subpopulation, indicating that these signaling pathways are more likely to specifically function in senescent tumor cells (Fig. 5c).

In the two major pathways, TGF-β can induce senescent phenotype of tumor cells, which is secreted by macrophages originating in tumor stroma[106, 107], and BMP is a family of TGF-β superfamily, which has similarly been found to induce senescence of tumor cells[108, 109]. Through signaling pathways pathway network, we found that senescent tumor cells receive TGF-β from macrophages (Fig. 5d), which is consistent with previous report in lymphoma[107]. Interestingly, senescent tumor cells received more TGF-β from cancer-associated fibroblasts (CAFs) (Fig. 5d). This may indicate that as a solid tumor, melanoma differs from lymphoma in microenvironment by the presence of a high number of fibroblasts. Moreover, senescent tumor cells received BMP from a variety of cell types in the microenvironment, of which the signal from T cells was the strongest (Fig. 5d). Further investigation of ligand-receptor interactions in signaling pathways revealed that the expression level of genes encoding receptors for TGF-β and BMP were higher in *senescent* subpopulation than in *cycling* and *transitional* subpopulations, with *TGFBR2* and *BMPR1B* showing more significant differences among these three subpopulations (Fig. 5e). In addition, survival analysis performed on TCGA-SKCM also showed that patients with higher expression level of *TGFBR1*, *TGFBR2* and *BMPR2* have better prognosis (Fig. 5f), consistent with the idea that stronger interactions by these pathways between senescent tumor cells and microenvironment could benefit patient survival.

We also noticed the other four signaling pathways which are also specific for senescent tumor cells. While *transitional* and *senescent* subpopulation interact with T cell by LEP signaling pathway and with CAFs by CSPG4 signaling pathway, the receptors involved in these two pathways did not show significant difference (Extended Data Fig.6a). Notably, *senescent* subpopulation interacts with T cell by CD6 signaling pathway and with macrophages by CCL signaling pathway. CD6 receptor encoding gene *ALMCAM* and CCL receptor encoding gene *CCR10* are specifically highly expressed in *senescent* subpopulation and benefit patients' survival (Extended Data Fig.6b, c). Although, these signaling pathways are reported associated with tumor progression[110-113], their functions on tumor cell senescence need further study. Overall, these results highlight the clinical value of hUSI in identifying senescent tumor cells and the potentially involved signaling pathways.

3 Methods

Data collection. Bulk RNA-seq datasets used for extraction of senescence features were collected from previously published papers[19-27]. We downloaded raw files from SRA database (https://www.ncbi.nlm.nih.gov/sra) (GSE53356, GSE56293, GSE58910, GSE61130, GSE63577, GSE64553, GSE113957, GSE130727, and GSE60883) and EMBL-EBI (https://www.ebi.ac.uk/ebisearch/about) (E-MTAB-5403). Only samples with confirmed senescence status were selected to build the representative senescence profiles. We also included corresponding non-senescent samples in each dataset for LOOCV. Seven microarray profiles used for batch effects test were download from Gene Expression Omnibus (GEO) database (https://www.ncbi.nlm.nih.gov/geo/) (GSE101750, GSE101758, GSE61130, GSE122079, GSE113060, GSE72407, and GSE72404). The RNA-seq and microarray profiles of independent validation datasets were also downloaded from SRA database through GEO accession numbers: GSE60340, GSE130306, GSE19864, GSE16058, GSE83922, GSE11954, GSE100014, and GSE77239. Four scRNA-seq profiles used for benchmarking were downloaded from GEO (GSE119807, GSE115301, GSE94980, and GSE81547). More details of datasets mentioned above can be found in Supplementary Table S1.

The TPM normalized gene expression matrix, of which, TCGA was collected from UCSC Xena (http://xena.ucsc.edu/public/), and GTEx was collected from GTEx Portal (version 8) (https://www.gtexportal.org/home/downloads/adult-gtex). The raw single-nuclei counts matrix of normal and COVID-19 patients' lung tissues and the processed melanoma profiles were also respectively downloaded from GEO under accession numbers GSE171524 and GSE72056.

Bulk RNA-seq data of training set processing. We used Prefetch v.3.0.2 to download SRA files and split them into FASTQ files by parallel-fastq-dump v.0.6.5. TrimGalore v.0.6.6 was used to filter out low quality reads and bases in 3' end for the consequential alignment performed by STAR v.2.2.1. We chose GRCh38 as reference genome sequence and only unique mapping reads were included. StringTie was used to qualify the gene expression level and normalize values by TPM (transcripts per million). Only protein coding genes (annotated by gencode v.31) with TPM >3 in 99% samples were included for next analysis. Considering bias introduced by batch effect, we also used log space transform to further reduce the disturbance for feature extraction.

Quantification of cellular senescence based on OCLR. To quantify CS based on gene expression level, a predictive model was built using OCLR[32] in R package “gelnet” with the parameters y=NULL, l1=0, and l2=1. The input expression matrix of senescent cells was normalized by subtracting mean expression value across all samples. The Spearman correlation coefficient was defined as hUSI as its stable performance for minimizing possible batch effects across datasets[114]. Normalized gene expression matrix was used to calculate hUSI.

Gene set enrichment analysis for learned-senescence features. Hallmark gene sets from The Molecular Signatures Database (MSigDB) database were included to perform GSEA for genes in OCLR learned-features which were sorted by their weights. Normalized enrichment score (NES) calculated by R package “fgsea”[115] was chosen to compare the enrichment degree in different gene sets.

Performance evaluation of hUSI. The reliability of the acquired feature and quantification strategy were validated using LOOCV. For each training round, we excluded one senescent sample in our training set and trained the model to extract senescence features. Then hUSI was calculated based on features to score the leave-out sample as well as all the non-senescent samples. Finally, the probability that the score of senescent samples is higher than that of non-senescent samples[116] was used to measure the performance, denoted as correctly ranking probability (CRP). For the four scRNA-seq datasets GSE119807, GSE115301, GSE94980, and GSE81547) used for comparison of three types of scoring methods, the expression matrix was read and normalized using R package “Seurat”. Then, log-normalized gene expression value was used for directly classifying senescent cells or calculating senescence score. ssGSEA score for each gene set was produced by “gsea()” function in the R package “GSVA”. To better compare the performance of all scoring methods in four single-cell datasets, we randomly divided each dataset into 10 subsets and repeated for 3 times by “createMultiFolds()” function in R package “caret”, finally generating 30 data units in total. For each of the 30 data units, we computed the AUC based on the scores generated by the tested methods described below by “auc()” function in R package “pROC”. For the expression level of marker genes, the parameter “direction” was not assigned as these genes were reported up or down regulated in senescent cells. For the computed senescence score and ssGSEA score, we set the parameter “direction=<” to make sure it will have a higher AUC only if these scores are lower in non-senescent samples. We calculated the average AUC of all 30 units and ascendingly ranked the average AUCs derived from each method group for each dataset. The mean average AUC rank across four datasets was used to reflect their overall performance (Supplementary Table S3).

Inference of cellular senescence states. For a large number of single cells, we adopted a GMM framework[117] to infer the number of potential senescence states according to the distribution of hUSI. Log transformation was firstly performed on the hUSI of each cell, that is, Logit(hUSI) = log2[(1+hUSI)/(1-hUSI)]. The Logit(hUSI) values of all cells were then fitted under the framework of GMM (implemented in R package “mclust”), and the Bayesian information criterion (BIC) was used to estimate the optimal number of senescence states and the probability that each cell belonged to a specific state[118].

Analysis of snRNA-seq data of COVID-19 infected samples. The raw expression matrix was read using Python module "scanpy" to filter out low quality cells (min_genes=200 and

min_cells=3). After removing mitochondrial and ribosomal genes, the expression matrix was normalized, and the highly variable gene matrix was considered for downstream scaling, batch effect removing and visualization. The "rpy2" module was used to call the "mclust" R package in python for cellular senescence state classification. GSEA for DEGs of senescence class was performed by python module “gseapy”[119] using $\log_2$-transformed Fold-Change as ranking metric.

Analysis of scRNA-seq data of melanoma samples. The processed melanoma single-cell matrices, retaining only defined tumor cells (malignant==2) and non-tumor cells (malignant==1) (including T-cells, B-cells, macrophages, endothelial cells, cancer-associated fibroblasts and natural killer cells), were read, analyzed and visualized using the R package "Seurat". To validate the reliability of inferred tumor subpopulations, specifically highly expressing genes (logfc.threshold > 0.1) of each subpopulation were overlapped with DEGs derived from melanoma microarray data (senescent vs young), which were calculated by linear models “lm(gene expession~pheno)”. R function “phyper()” was used to test the overlapping significance. To observe the positional relationships of the different subpopulations of CS states on projected space, for each gene, we calculated the Pearson correlation coefficient between hUSIs and gene expression values of all cells, and the top 1500 genes ranked by absolute correlation coefficient values were selected as hUSI related genes. Then, using the tool ICAnet[120], the tumor cells were integrated based on the 38 co-expression modules of the above hUSI related genes. Diffusion map based on five principal components of 38 co-expression modules was used to further reduce the dimension and infer senescence trajectory using R package “destiny”[121]. Specifically highly expressed genes (logfc.threshold > 0.1) of tumor subpopulation were enriched using R package “clusterProfiler ”[122] on the database Gene-Ontology (GO), Kyoto Encyclopedia of Genes and Genomes (KEGG), using $\log_2$-transformed Fold-Change as the ranking metric. Cell communication analysis was carried out using R package “CellChat”, and the communication intensity between tumor subpopulations and different non-tumor cell types in a signal network was quantified[105]. When filtered pathways specific for senescent tumor cells, we set three tumor subpopulations as “target” and T cell, NK cell, macro cell and CAF cell as “source”.

Data analysis of melanoma patient cohort in TCGA. The normalized Level 3 RNA-seq data of a melanoma patient cohort (SKCM) with associated clinical data were downloaded from the TCGA (the Cancer Genome Atlas) database using R package TCGAbiolinks[123]. To analyze the proportion of cells with different senescence degree, three tumor subpopulations were used as reference to deconvolute the RNA-seq data of the SKCM patient cohort using EpiDISH[99]. The abundance of the 22 immune components were calculated by CIBERSORT[100]. Survival analysis was performed using R packages “survival” and “survminer” with “OS = vital_status” and “OS.time = days_to_last_followup”.

4 Discussion

Though the characterization, identification, and pharmacological clearance of senescent cell are the basics of many senotherapies, the relative scarce of specific and efficient senescence marker keeps limiting the study of distinguishing and targeting senescent cells both *in vitro* and *in vivo*[1, 10, 124, 125]. Additionally, in single-cell studies, the differential

expression level of a single senescence marker is insufficient to identify senescent cells due to the heterogeneity of both cell types and senescence status[64]. Besides, apart from the absence or low expression of certain senescence markers, the possibility of improperly calculating senescence score in some methods also exists due to the absent detection or abnormal expression of key senescence genes. For example, in lassoCS[18] method, three out of ten genes (*SEMA3G*, *PCSK6*, and *SLC44A4*) are assigned with weight values for senescence score calculation, while they are absent when we applied it to another single-cell dataset[48]. Taking gene sets into consideration, while the enrichment score generated by GSEA or GSVA is widely utilized, different gene sets usually emphasize on different aspects of senescence. For instance, the SASP gene set focuses on the activated secretory phenotype, whereas signature of replicative senescence[76] specifically considers replicative-related changes. Notably, performing GSEA in large-scale single-cell atlases can be exceedingly time-consuming, due to the substantial number of permutations required to accurately estimate the nominal p-value[126].

To overcome these challenges above, the present study adopted OCLR machine learning algorithm[32] to acquire gene expression features of CS in relatively comprehensive senescence transcriptome profiles. Based on OCLR machine learned-features, we developed hUSI, a scoring method using Spearman correlation coefficient that can distinguish senescent samples or cells induced by different factors while less affected by batch effect. We validated the generalizability of hUSI by applying it to datasets of variety origins encompassing platforms, cell types, or induction factors that were not included in the training set. Moreover, the stability and the potential application of hUSI on single-cell data were further validated by simulated sparse profiles and real scRNA-seq profiles.

Comparing with other currently available methods (including those based on senescence markers expression level, computed senescence score and ssGSEA score), hUSI manifested its reliability and superior performance in senescence evaluation. Unlike methods that rely on limited genes, hUSI takes14,638 protein-coding genes assigned with different weights learned by OCLR into senescence evaluation, which reduces bias when evaluating CS of distinct senescence types. Importantly, hUSI demonstrated reliable performance when applied to samples derived from both health and disease populations.

Combination of hUSI with GMM provided a framework to reveal cell classes with different senescence level. hUSI identified sell types showing higher accumulation of senescent cells in COVID-19-infected lung tissue and provided a potential therapeutic avenue for selectively eliminating these senescent cells to mitigate senescence-induced hyperinflammation in COVID-19 patients[82]. For example, navitoclax, a senolytic drug, has been reported to target senescent alveolar epithelial cells and macrophages, and in turn reduces the secretion of pro-inflammatory SASP factors after SARS-CoV-2 infection[81]. Thus, our ongoing research will center on integrating senescence quantification into the cellular response to drugs to unveil the contribution of senescent cells to both drug resistance and drug sensitivity across various diseases.

By investigating the communication network of melanoma cells of different senescence degree, combing with previous studies[106, 107], we hypothesize that senescent tumor cells can interact with tumor microenvironment by TGF-β and BMP signaling pathways in melanoma microenvironment and contribute to anti-cancer effects. TGF-β is well known

being associated with the upregulated expression of p15, p21, and p27, which are known senescence markers and can inhibit cell proliferation[127]. BMP, a member of TGF-β family, has also been reported having a crucial role in paracrine induction in senescent cells[108, 109]. We observed higher expression level of genes encoding TGF and BMP receptors in senescent cells, which support their specifical functions in senescence of tumor cells.

Although hUSI has demonstrated superior performance in multiple aspects, we must admit that there are still some limitations in current status. First, though the stability of hUSI has been demonstrated by LOOCV and independent datasets, with more data coming in the big data era, the quality and quantity of training sets still has room for further improvement to optimize the performance of hUSI in the future. Second, cell-cell interactions networks are dynamic and intricate, no matter among senescent cells in different cell types or between senescent cells and non-senescent cells. However, in this study, we simplified the interactions networks by only focusing on senescent tumor cells due to the limited cell numbers of other cell types. Besides, the causal relationship between signaling pathways and the mechanism of how senescent tumor cells response to different signals also require further study. Third, hUSI was a human transcriptome-based scoring method. Although, using homologous genes when applied to other species is a feasible way, the reliability and the accuracy need extensive validation. We also believed senescence scoring tool can be developed based on transcriptomes of interested species following our stagey. Finally, with implementation of quantifying CS degree, a more detailed and standardized CS atlas supported by adequate experimental and multi-omics evidence is demanding to benefit the prevention of aging-related diseases and the application of senotherapeutics.

5 Conclusion

In summary, we developed a senescence-evaluating tool that outperforms currently existing analogous methods, capable of robustly quantifying sample senescence degree based on bulk or single-cell transcriptome profiles. We also proposed a framework for classifying the senescence status of various cell types and recognizing senescence-specific intercellular communications. Based on the outperformance and applicability of hUSI, we believe that it will greatly help to evaluate senescence and benefit studies and even therapeutic strategies in senescence and age-related diseases.

6 Declarations

Funding

This work was financially supported by the National Natural Science Foundation of China (92249302, 32370592), the National Key Research and Development Program of China (2023YFC3603300, 2021YFA0909300).

Conflict of interest

The authors declare no competing interests.

Code availability

hUSI can be implemented both in R and Python, the data and codes used to reproduce our analysis results are provided in GitHub (https://github.com/WJPina/HUSI), along with a detailed usage guideline.

Author contribution
The manuscript was written by J.W., W.W., and J.Y. and polished by G.W., and T.N.. The method was conceived by J.Y. and W.W. and the algorithm is implemented by J.W., and J.Y. Computational analyses and algorithm evaluations were conducted by J.W., W.W., J.Y., and X.Z. This work was supervised by T.N..

7 Extended Data

Extended Data Fig.1

Information of training and validation data.

Extended Data Fig.2

hUSI enables to distinguish senescent samples in complete and zeroing-out microarray profiles.

Extended Data Fig.3

Comparison of three types of senescence qualification methods in four scRNA-seq datasets.

Extended Data Fig.4

hUSI enables to uncover senescent cells accumulated in COVID-19 lung tissues.

Extended Data Fig.5

hUSI enables to distinguish senescent tumor cells in melanoma.

Extended Data Fig.6

Signal pathways are specific for senescent tumor cells.

8 Supplementary information

Supplementary Table 1

Details of datasets used for training model, validation and evaluation.

Supplementary Table 2

Details of learned-senescence features.

Supplementary Table 3

AUC results of methods included in comparison.

Supplementary Table 4

Eight gene sets included in comparison.

Supplementary Table 5

DEGs in melanoma microarray data and specific highly expressed genes of three tumor subpopulations in melanoma scRNA-seq data.

9 Main figures

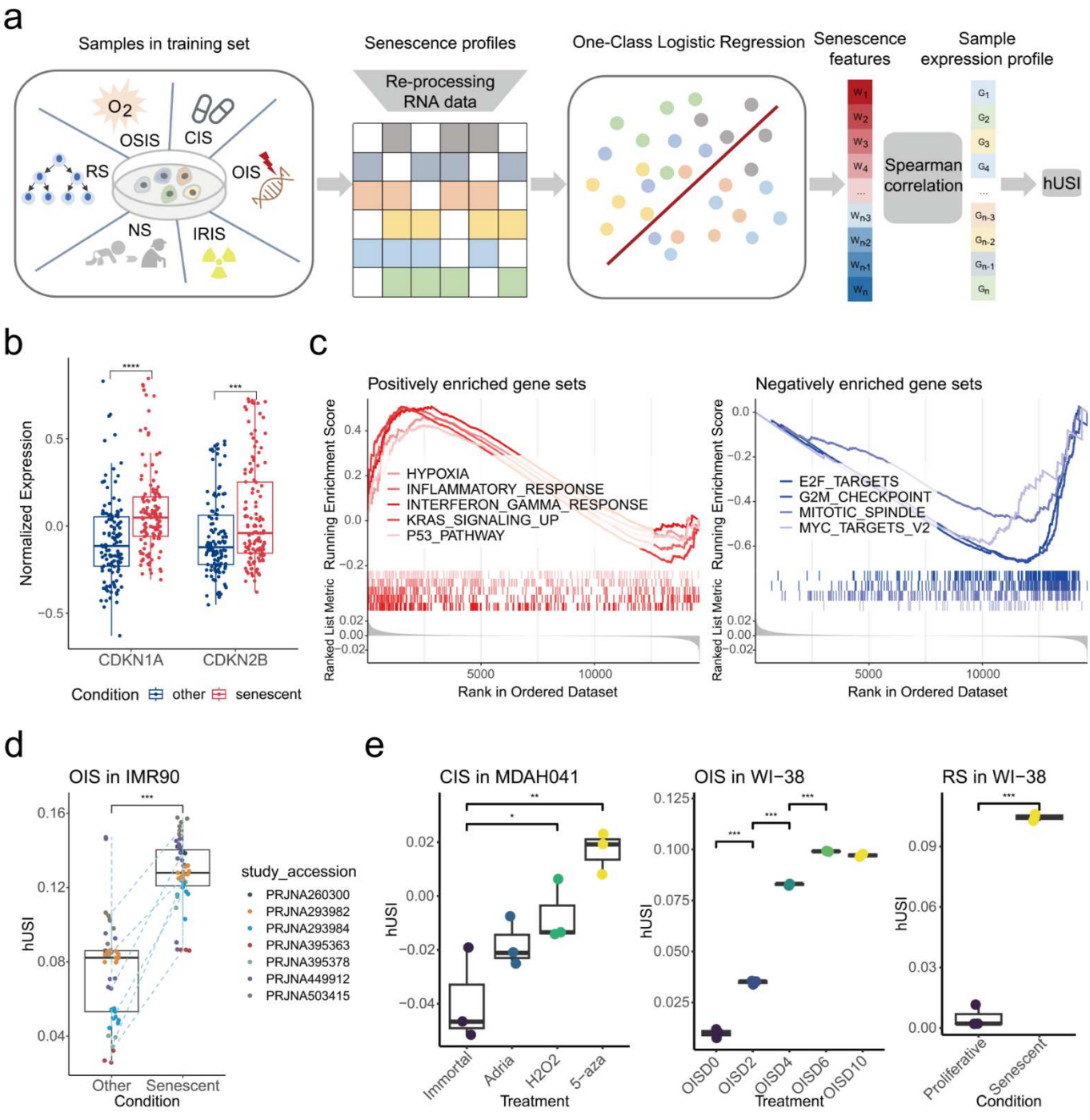

Fig.1|Training and validation of hUSI. a. Development workflow of hUSI. First, RNA-seq data sets derived from five cell types and six senescence inducing factors were included in the training datasets. Second, senescence profiles were re-processed by a unified RNA-seq data processing pipeline. Third, OCLR was chosen to learn the senescence features, generating a weighted gene set. Finally, Spearman correlation coefficient between weights and expression values of genes is defined as hUSI. **b.** Senescent samples in training set have significant higher expression level of *CDKN1A* and *CDKN2B* than corresponding non-senescent samples (**** means p<1e-4 and *** means p<1e-3, *t*-test with Bonferroni correction). **c.** Senescence features learned by OCLR were significantly positively enriched in senescence associated gene sets (left panel) and negatively enriched in proliferation gene sets (right panel). Each line represents a different hallmark gene set with a variety of color shade of line depending on normalized enrichment sore (NSE). **d.** Senescent samples showed significant higher hUSIs than non-senescent (normal or proliferative) samples across seven studies, which demonstrated hUSI is robust against batch effects (*** means p<1e-3, one-tail *t*-test). Dotted lines represent paired senescent and control samples. **e.** hUSIs of senescent samples caused by CIS, OIS and RS in MDAH04 or WI-38 cell lines are all significantly higher than corresponding control samples (* means p<0.05, ** means p<0.01 and *** means p<1e-3, one-tail *t*-test).

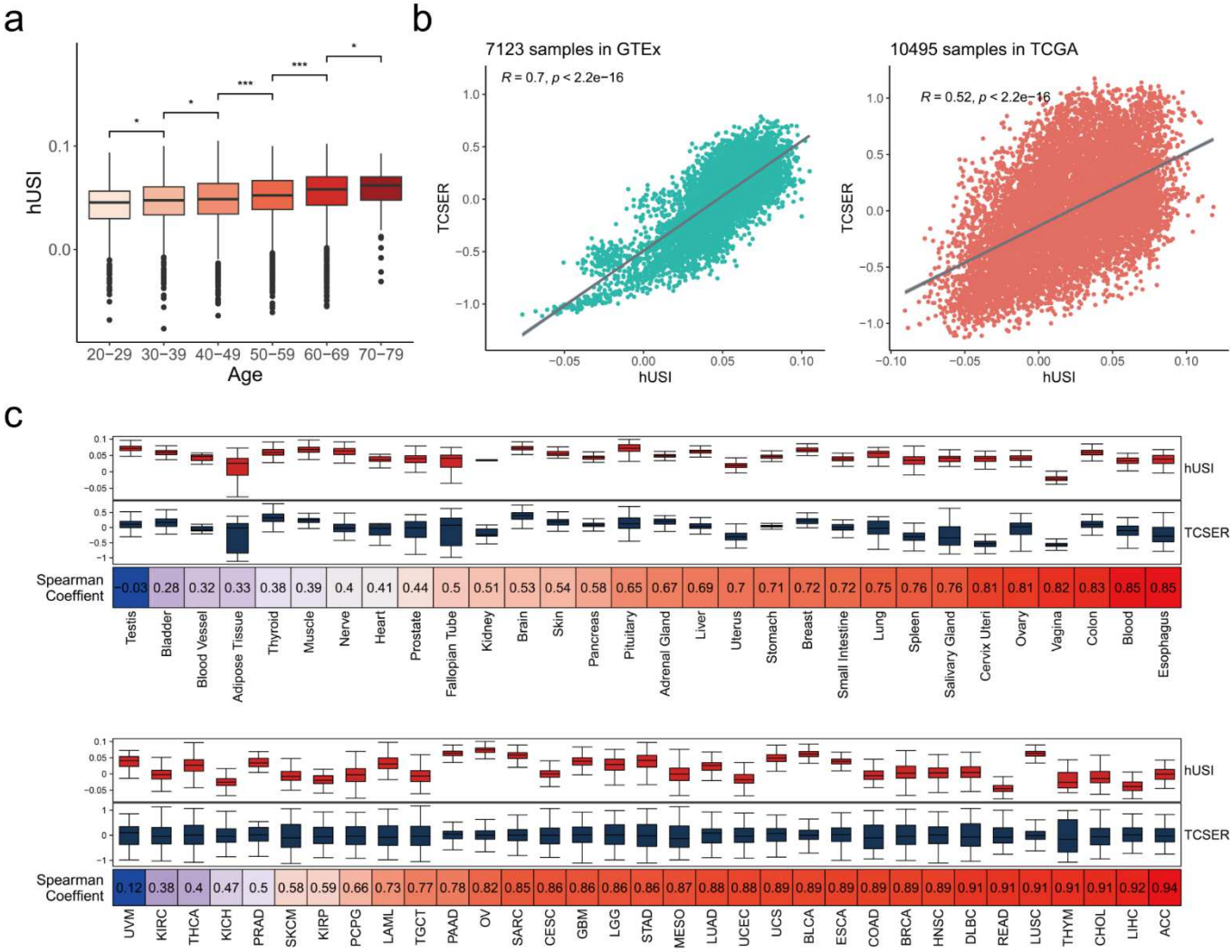

Fig.2|hUSI gives reliable senescence evaluation for samples from GTEx and TCGA. **a.** hUSIs progressively elevate with increased donor age for GTEx samples (* means p<0.05, ** means p<0.01 and *** means p<1e-3, one-tail *t*-test). **b.** hUSIs are significantly positively correlated with CS scores in both GTEx (left panel) and TCGA (right panel) samples. Spearman correlation coefficients (denoted as R values) were used for the evaluation. **c.** hUSIs and CS scores present high Spearman coefficients in most tissues (GTEx, upper panel) and cancer types (TCGA, lower panel).

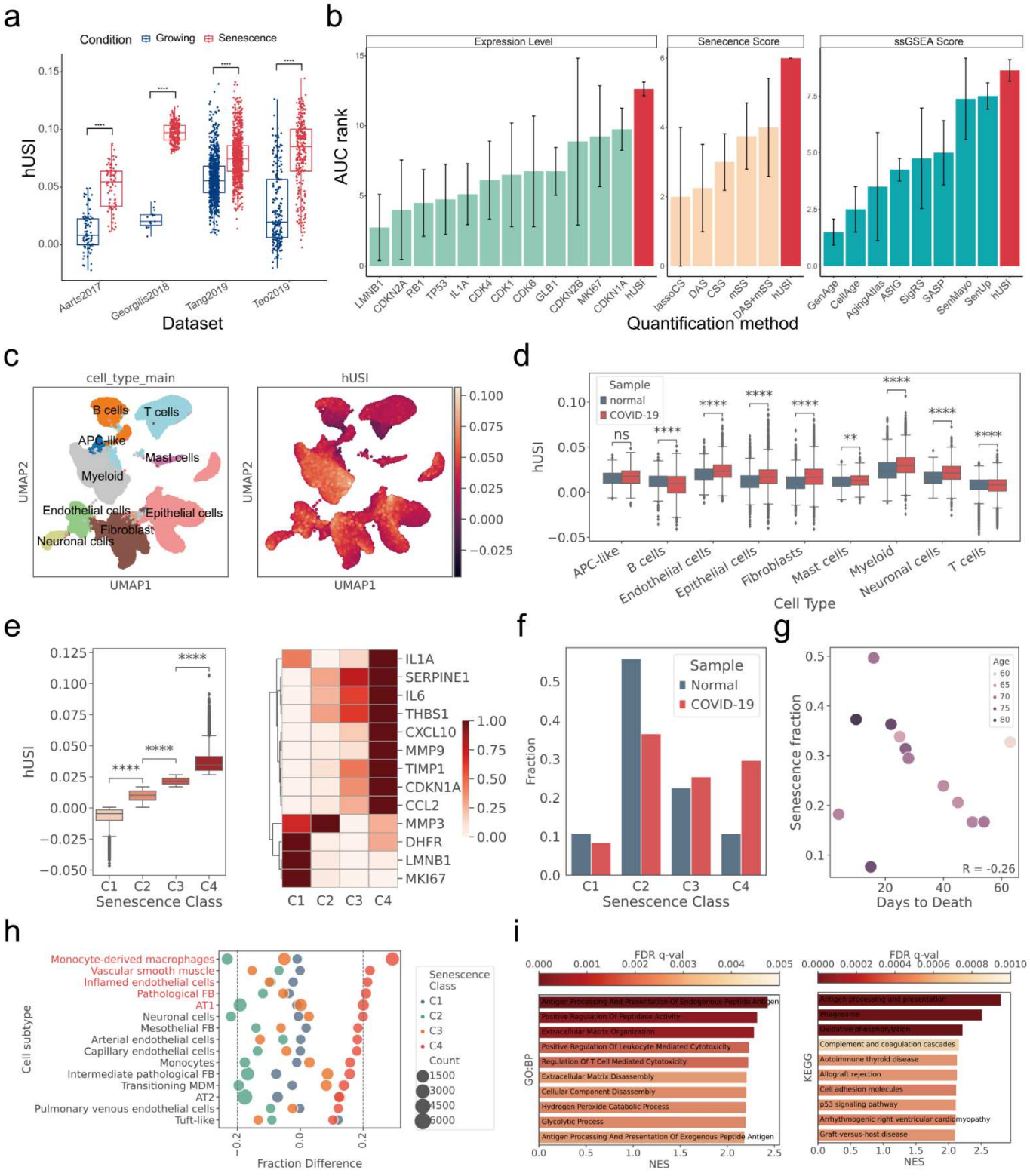

Fig.3|hUSI enable to distinguish senescent cells in various conditions. a. hUSIs are significantly higher in senescent cells than growing cells across four single-cell datasets (**** means p<1e-4, *t*-test). **b.** AUC rank shows hUSI outperformed 12 senescence or proliferation marker genes, five methods and eight senescence-associated gene sets in

evaluating senescence status. Marker gene expression value, computed senescence score and ssGSEA score are respectively used to calculate AUC on four scRNA-seq datasets. Error bars were based on the AUC ranks across four single-cell datasets. **c.** hUSI distribution of nine annotated cell types in the snRNA-seq dataset collected from COVID-19-infected lung tissues. **d**. Epithelial cells, endothelial cells, fibroblasts, myeloid, and neuronal cells from COVID-19 patients exhibited significantly higher hUSIs compared to normal donors (**** denote p<1e-4, Mann-Whitney tests followed by Bonferroni corrections). **e.** Cells can be divided into four classes with significantly different senescence degree (C1~C4) (**** denote p<1e-4, Mann-Whitney tests followed by Bonferroni corrections) and the most senescent cells (C4) have apparent higher expression levels of core senescence- and SASP-related genes and lower expression level of proliferation-related genes. **f.** Lung tissue from COVID-19 patients has a higher fraction of C4 than normal sample. **g.** Higher fraction of senescent cells (C4) (y-axis) existed in COVID-19 patients with less days from symptom onset to death (x-axis). The spearman correlation coefficient (denoted as R) between days to death and C4 fraction is -0.26. **h.** Top 15 cell types which display higher fraction of senescent cells (C4) in COVID-19 lungs comparing to normal lungs. Top five cell types were highlighted whose fraction difference is larger than 0.2. **i.** Using GSEA, DEGs of senescent AT1 cells (C4 vs C2) were enriched on GO terms (Biological process) and KEEG terms. Top ten terms were plotted (sorted by NES), all terms have false discovery rate (FDR) less than 0.005.

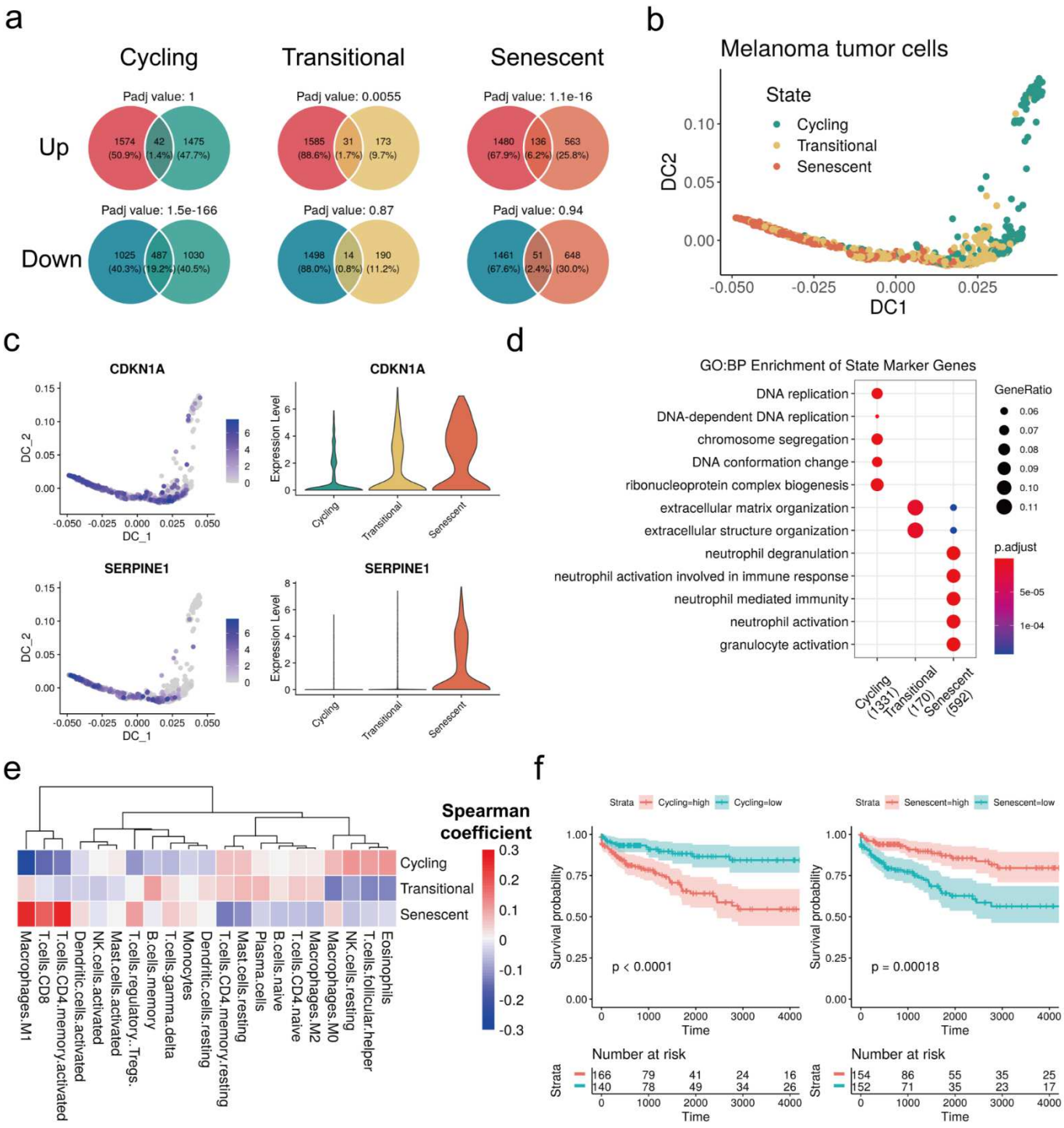

Fig.4|Identifying senescent tumor cells to benefit patient survival. a. Validating the senescence degrees of *cycling*, *transitional* and *senescent* subpopulations by overlap comparison with DEGs (up or down regulated) in bulk samples (senescence vs growing). Hypergeometric distribution test was used to calculate the p values. **b.** Diffusion map showing a trajectory from *cycling* cells to *senescent* cells in melanoma. **c.** Two classical aging-related marker genes (*CDKN1A* and *SERPINE*) showed increased expression level along trajectory and in senescent subpopulation. **d.** Different GO terms (biological process)

characterize *cycling*, *transitional* and *senescent* subpopulations, with *replication-associated* terms enriched in *cycling* subpopulation while *immunity activation*-related terms enriched in *senescent* subpopulation. **e.** Heatmap of Spearman correlation coefficient between the three subpopulations and the abundance of 22 immune cell types indicates that senescent tumor cells were associated with immunity activation. **f.** Survival curves of melanoma patients with different proportion of *cycling* and *senescent* cell subpopulations.

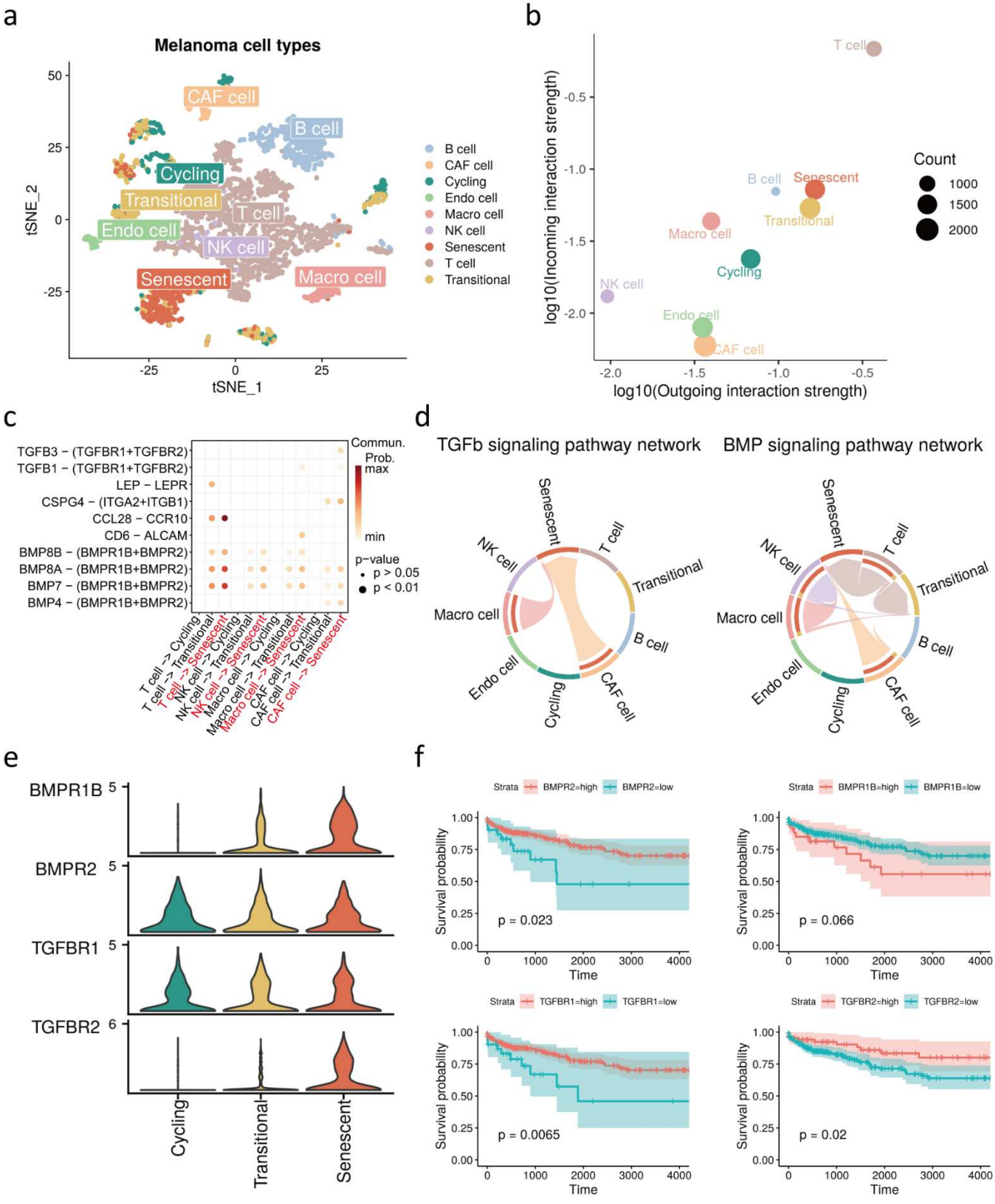
a
Melanoma cell types
CAF cell
B cell
Cycling
Transitional
T cell
Endo cell
NK cell
Senescent
Macro cell
tSNE_1
tSNE_2
B cell
CAF cell
Cycling
Endo cell
Macro cell
NK cell
Senescent
T cell
Transitional
b
log10(Incoming interaction strength)
log10(Outgoing interaction strength)
Count
1000
1500
2000
c
Commun. Prob.
max
min
p−value
p > 0.05
p < 0.01
TGFB3 − (TGFBR1+TGFBR2)
TGFB1 − (TGFBR1+TGFBR2)
LEP − LEPR
CSPG4 − (ITGA2+ITGB1)
CCL28 − CCR10
CD6 − ALCAM
BMP8B − (BMPR1B+BMPR2)
BMP8A − (BMPR1B+BMPR2)
BMP7 − (BMPR1B+BMPR2)
BMP4 − (BMPR1B+BMPR2)
d
TGFb signaling pathway network
BMP signaling pathway network
e
BMPR1B
BMPR2
TGFBR1
TGFBR2
Cycling
Transitional
Senescent
f
Strata
BMPR2=high
BMPR2=low
p = 0.023
BMPR1B=high
BMPR1B=low
p = 0.066
TGFBR1=high
TGFBR1=low
p = 0.0065
TGFBR2=high
TGFBR2=low
p = 0.02
Survival probability
Time

Fig.5|TNF-β and BMP signal pathways are specific for senescent tumor cells. a. Three subpopulations of tumor cells and other six cell types presented in tumor microenvironment (T cell, B cell, natural killer (NK) cell, macrophage (Macro) cell, endothelial (Endo) cell and CAFs) are taken to infer cell-cell communications in tumor microenvironment. **b.** The *Senescent* subpopulation exhibits higher interaction strength than other two subpopulations (*cycling* and *transitional*). X-axis and y-axis represent $\log_{10}$-transformed outgoing and incoming interaction strength, respectively. **c.** Ten ligand-receptor pairs showing specifically high communication probability in *senescent* subpopulation, with two pairs belonging to TNF-β signaling pathway and four pairs belonging to BMP signal pathway. **d.** *Senescent* subpopulation receives TGF-β and BMP signals mainly from CAFs and T cell in cell-cell communication networks. **e.** *Senescent* subpopulation shows higher expression level of gene encoding receptors involved in TGF-β (*TGFBR1* and *TGFBR1*) and BMP (*BMPR1B* and *BMPR2*) signaling pathways. **f.** Melanoma patients with high expression level of *BMPR2*, *TGFBR1* or *TGFBR1* have a significant better survival prognosis.

10 References

1. van Deursen, J.M. The role of senescent cells in ageing. *Nature* **509**, 439-46 (2014).
2. Acosta, J.C. et al. A complex secretory program orchestrated by the inflammasome controls paracrine senescence. *Nat Cell Biol* **15**, 978-90 (2013).
3. Birch, J. & Gil, J. Senescence and the SASP: many therapeutic avenues. *Genes Dev* **34**, 1565-1576 (2020).
4. Chaib, S., Tchkonia, T. & Kirkland, J.L. Cellular senescence and senolytics: the path to the clinic. *Nat Med* **28**, 1556-1568 (2022).
5. Wang, L., Lankhorst, L. & Bernards, R. Exploiting senescence for the treatment of cancer. *Nat Rev Cancer* **22**, 340-355 (2022).
6. Cho, K.A. et al. Morphological adjustment of senescent cells by modulating caveolin-1 status. *J Biol Chem* **279**, 42270-8 (2004).
7. Petrova, N.V., Velichko, A.K., Razin, S.V. & Kantidze, O.L. Small molecule compounds that induce cellular senescence. *Aging Cell* **15**, 999-1017 (2016).
8. Rossiello, F., Herbig, U., Longhese, M.P., Fumagalli, M. & D'Adda, D.F.F. Irreparable telomeric DNA damage and persistent DDR signalling as a shared causative mechanism of cellular senescence and ageing. *Curr Opin Genet Dev* **26**, 89-95 (2014).
9. Munoz-Espin, D. et al. Programmed cell senescence during mammalian embryonic development. *Cell* **155**, 1104-18 (2013).
10. Hernandez-Segura, A., Nehme, J. & Demaria, M. Hallmarks of Cellular Senescence. *Trends Cell Biol* **28**, 436-453 (2018).
11. Huang, W., Hickson, L.J., Eirin, A., Kirkland, J.L. & Lerman, L.O. Cellular senescence: the good, the bad and the unknown. *Nature reviews. Nephrology* **18**, 611-627 (2022).
12. Han, X. et al. Construction of a human cell landscape at single-cell level. *Nature* **581**, 303-309 (2020).
13. He, S. et al. Single-cell transcriptome profiling of an adult human cell atlas of 15 major organs. *Genome Biol* **21**, 294 (2020).
14. Lafferty-Whyte, K. et al. Scoring of senescence signalling in multiple human tumour gene expression datasets, identification of a correlation between senescence score and drug toxicity in the NCI60 panel and a pro-inflammatory signature correlating with survival advantage in peritoneal mesothelioma. *BMC Genomics* **11**, 532 (2010).

15. de Magalhaes, J.P., Curado, J. & Church, G.M. Meta-analysis of age-related gene expression profiles identifies common signatures of aging. *Bioinformatics* **25**, 875-81 (2009).
16. Saul, D. et al. A new gene set identifies senescent cells and predicts senescence-associated pathways across tissues. *Nat Commun* **13**, 4827 (2022).
17. Wang, X. et al. Comprehensive assessment of cellular senescence in the tumor microenvironment. *Brief Bioinform* **23** (2022).
18. Gong, Q., Jiang, Y., Xiong, J., Liu, F. & Guan, J. Integrating scRNA and bulk-RNA sequencing develops a cell senescence signature for analyzing tumor heterogeneity in clear cell renal cell carcinoma. *Front Immunol* **14**, 1199002 (2023).
19. Hernandez-Segura, A. et al. Unmasking Transcriptional Heterogeneity in Senescent Cells. *Curr Biol* **27**, 2652-2660.e4 (2017).
20. Casella, G. et al. Transcriptome signature of cellular senescence. *Nucleic Acids Res* **47**, 7294-7305 (2019).
21. Rai, T.S. et al. HIRA orchestrates a dynamic chromatin landscape in senescence and is required for suppression of neoplasia. *Genes Dev* **28**, 2712-25 (2014).
22. Alspach, E. et al. P38MAPK plays a crucial role in stromal-mediated tumorigenesis. *Cancer discovery* **4**, 716
-729
(2014).
23. Crowe, E.P. et al. Changes in the Transcriptome of Human Astrocytes Accompanying Oxidative Stress-Induced Senescence. *Front Aging Neurosci* **8**, 208 (2016).
24. Herranz, N. et al. mTOR regulates MAPKAPK2 translation to control the senescence-associated secretory phenotype. *Nat Cell Biol* **17**, 1205-17 (2015).
25. Marthandan, S. et al. Similarities in Gene Expression Profiles during In Vitro Aging of Primary Human Embryonic Lung and Foreskin Fibroblasts. *Biomed Res Int* **2015**, 731938 (2015).
26. Marthandan, S. et al. Hormetic effect of rotenone in primary human fibroblasts. *Immun Ageing* **12**, 11 (2015).
27. Fleischer, J.G. et al. Predicting age from the transcriptome of human dermal fibroblasts. *Genome Biol* **19**, 221 (2018).
28. Lin, W. et al. Identification and validation of cellular senescence patterns to predict clinical outcomes and immunotherapeutic responses in lung adenocarcinoma. *Cancer Cell Int* **21**, 652 (2021).
29. Park, H.S. & Kim, S.Y. Endothelial cell senescence: A machine learning-based meta-analysis of transcriptomic studies. *Ageing Res Rev* **65**, 101213 (2021).
30. Jochems, F. et al. The Cancer SENESCopedia: A delineation of cancer cell senescence. *Cell Rep* **36**, 109441 (2021).
31. Kumari, R. & Jat, P. Mechanisms of Cellular Senescence: Cell Cycle Arrest and Senescence Associated Secretory Phenotype. *Front Cell Dev Biol* **9**, 645593 (2021).
32. Sokolov, A., Paull, E.O. & Stuart, J.M. ONE-CLASS DETECTION OF CELL STATES IN TUMOR SUBTYPES. *Pac Symp Biocomput* **21**, 405-16 (2016).
33. Lim, S., Lim, J., Lee, A., Kim, K.I. & Lim, J.S. Anticancer Effect of E26 Transformation-Specific Homologous Factor through the Induction of Senescence and the Inhibition of Epithelial-Mesenchymal Transition in Triple-Negative Breast Cancer Cells. *Cancers (Basel)* **15** (2023).
34. Takaya, K., Asou, T. & Kishi, K. Identification of Apolipoprotein D as a Dermal Fibroblast Marker of Human Aging for Development of Skin Rejuvenation Therapy. *Rejuvenation Res* **26**, 42-50 (2023).
35. Hari, P. et al. The innate immune sensor Toll-like receptor 2 controls the senescence-associated secretory phenotype. *Sci Adv* **5**, eaaw0254 (2019).

36. Liberzon, A. et al. The Molecular Signatures Database (MSigDB) hallmark gene set collection. *Cell Syst* **1**, 417-425 (2015).
37. Kim, K.S., Kang, K.W., Seu, Y.B., Baek, S.H. & Kim, J.R. Interferon-gamma induces cellular senescence through p53-dependent DNA damage signaling in human endothelial cells. *Mech Ageing Dev* **130**, 179-88 (2009).
38. Cisowski, J., Sayin, V.I., Liu, M., Karlsson, C. & Bergo, M.O. Oncogene-induced senescence underlies the mutual exclusive nature of oncogenic KRAS and BRAF. *Oncogene* **35**, 1328-33 (2016).
39. Lasry, A. & Ben-Neriah, Y. Senescence-associated inflammatory responses: aging and cancer perspectives. *Trends Immunol* **36**, 217-28 (2015).
40. Artandi, S.E. & Attardi, L.D. Pathways connecting telomeres and p53 in senescence, apoptosis, and cancer. *Biochem Biophys Res Commun* **331**, 881-90 (2005).
41. Serrano, M., Lin, A.W., McCurrach, M.E., Beach, D. & Lowe, S.W. Oncogenic ras provokes premature cell senescence associated with accumulation of p53 and p16INK4a. *Cell* **88**, 593-602 (1997).
42. Oshi, M. et al. G2M Cell Cycle Pathway Score as a Prognostic Biomarker of Metastasis in Estrogen Receptor (ER)-Positive Breast Cancer. *Int J Mol Sci* **21** (2020).
43. Narita, M. et al. Rb-mediated heterochromatin formation and silencing of E2F target genes during cellular senescence. *Cell* **113**, 703-16 (2003).
44. Dikovskaya, D. et al. Mitotic Stress Is an Integral Part of the Oncogene-Induced Senescence Program that Promotes Multinucleation and Cell Cycle Arrest. *Cell Rep* **12**, 1483-96 (2015).
45. Wu, C.H. et al. Cellular senescence is an important mechanism of tumor regression upon c-Myc inactivation. *Proc Natl Acad Sci U S A* **104**, 13028-33 (2007).
46. Guerrero, A. et al. Cardiac glycosides are broad-spectrum senolytics. *Nat Metab* **1**, 1074-1088 (2019).
47. Hoare, M. et al. NOTCH1 mediates a switch between two distinct secretomes during senescence. *Nat Cell Biol* **18**, 979-92 (2016).
48. Parry, A.J. et al. NOTCH-mediated non-cell autonomous regulation of chromatin structure during senescence. *Nat Commun* **9**, 1840 (2018).
49. Georgilis, A. et al. PTBP1-Mediated Alternative Splicing Regulates the Inflammatory Secretome and the Pro-tumorigenic Effects of Senescent Cells. *Cancer Cell* **34**, 85-102.e9 (2018).
50. Costarelli, L. et al. Different transcriptional profiling between senescent and non-senescent human coronary artery endothelial cells (HCAECs) by Omeprazole and Lansoprazole treatment. *Biogerontology* **18**, 217-236 (2017).
51. Chicas, A. et al. Dissecting the unique role of the retinoblastoma tumor suppressor during cellular senescence. *Cancer Cell* **17**, 376-87 (2010).
52. Orfanidis, K., Waster, P., Lundmark, K., Rosdahl, I. & Ollinger, K. Evaluation of tubulin beta-3 as a novel senescence-associated gene in melanocytic malignant transformation. *Pigment Cell Melanoma Res* **30**, 243-254 (2017).
53. Garbe, J.C. et al. Molecular distinctions between stasis and telomere attrition senescence barriers shown by long-term culture of normal human mammary epithelial cells. *Cancer Res* **69**, 7557-68 (2009).
54. Krizhanovsky, V. et al. Senescence of activated stellate cells limits liver fibrosis. *Cell* **134**, 657-67 (2008).
55. Yuan, L. et al. Switching off IMMP2L signaling drives senescence via simultaneous metabolic alteration and blockage of cell death. *Cell Res* **28**, 625-643 (2018).

56. Somekh, J., Shen-Orr, S.S. & Kohane, I.S. Batch correction evaluation framework using a-priori gene-gene associations: applied to the GTEx dataset. *BMC Bioinformatics* **20**, 268 (2019).
57. Purcell, M., Kruger, A. & Tainsky, M.A. Gene expression profiling of replicative and induced senescence. *Cell Cycle* **13**, 3927-37 (2014).
58. Sati, S. et al. 4D Genome Rewiring during Oncogene-Induced and Replicative Senescence. *Mol Cell* **78**, 522-538.e9 (2020).
59. Borghesan, M., Hoogaars, W., Varela-Eirin, M., Talma, N. & Demaria, M. A Senescence-Centric View of Aging: Implications for Longevity and Disease. *Trends Cell Biol* **30**, 777-791 (2020).
60. Aarts, M. et al. Coupling shRNA screens with single-cell RNA-seq identifies a dual role for mTOR in reprogramming-induced senescence. *Genes Dev* **31**, 2085-2098 (2017).
61. Tang, H. et al. Single senescent cell sequencing reveals heterogeneity in senescent cells induced by telomere erosion. *Protein Cell* **10**, 370-375 (2019).
62. Teo, Y.V. et al. Notch Signaling Mediates Secondary Senescence. *Cell Rep* **27**, 997-1007.e5 (2019).
63. Minamino, T. et al. A crucial role for adipose tissue p53 in the regulation of insulin resistance. *Nat Med* **15**, 1082-7 (2009).
64. Wiley, C.D. et al. Analysis of individual cells identifies cell-to-cell variability following induction of cellular senescence. *Aging Cell* **16**, 1043-1050 (2017).
65. Orjalo, A.V., Bhaumik, D., Gengler, B.K., Scott, G.K. & Campisi, J. Cell surface-bound IL-1alpha is an upstream regulator of the senescence-associated IL-6/IL-8 cytokine network. *Proc Natl Acad Sci U S A* **106**, 17031-6 (2009).
66. Diril, M.K. et al. Cyclin-dependent kinase 1 (Cdk1) is essential for cell division and suppression of DNA re-replication but not for liver regeneration. *Proc Natl Acad Sci U S A* **109**, 3826-31 (2012).
67. Alessio, N. et al. Different Stages of Quiescence, Senescence, and Cell Stress Identified by Molecular Algorithm Based on the Expression of Ki67, RPS6, and Beta-Galactosidase Activity. *Int J Mol Sci* **22** (2021).
68. Kansara, M. et al. Immune response to RB1-regulated senescence limits radiation-induced osteosarcoma formation. *J Clin Invest* **123**, 5351-60 (2013).
69. McConnell, B.B., Starborg, M., Brookes, S. & Peters, G. Inhibitors of cyclin-dependent kinases induce features of replicative senescence in early passage human diploid fibroblasts. *Curr Biol* **8**, 351-4 (1998).
70. Liu, S. et al. Senescence of human skin-derived precursors regulated by Akt-FOXO3-p27(KIP(1))/p15(INK(4)b) signaling. *Cell Mol Life Sci* **72**, 2949-60 (2015).
71. Lee, B.Y. et al. Senescence-associated beta-galactosidase is lysosomal beta-galactosidase. *Aging Cell* **5**, 187-95 (2006).
72. Tacutu, R. et al. Human Ageing Genomic Resources: new and updated databases. *Nucleic Acids Res* **46**, D1083-D1090 (2018).
73. Saul, D. & Kosinsky, R.L. Single-Cell Transcriptomics Reveals the Expression of Aging- and Senescence-Associated Genes in Distinct Cancer Cell Populations. *Cells* **10** (2021).
74. Aging Atlas: a multi-omics database for aging biology. *Nucleic Acids Res* **49**, D825-D830 (2021).
75. Chatsirisupachai, K., Palmer, D., Ferreira, S. & de Magalhaes, J.P. A human tissue-specific transcriptomic analysis reveals a complex relationship between aging, cancer, and cellular senescence. *Aging Cell* **18**, e13041 (2019).
76. Reyfman, P.A. et al. Single-Cell Transcriptomic Analysis of Human Lung Provides Insights into the Pathobiology of Pulmonary Fibrosis. *Am J Respir Crit Care Med* **199**, 1517-1536 (2019).

77. Nehme, J., Borghesan, M., Mackedenski, S., Bird, T.G. & Demaria, M. Cellular senescence as a potential mediator of COVID-19 severity in the elderly. *Aging Cell* **19**, e13237 (2020).
78. Lipskaia, L. et al. Evidence That SARS-CoV-2 Induces Lung Cell Senescence: Potential Impact on COVID-19 Lung Disease. *Am J Respir Cell Mol Biol* **66**, 107-111 (2022).
79. Melms, J.C. et al. A molecular single-cell lung atlas of lethal COVID-19. *Nature* **595**, 114-119 (2021).
80. Bartleson, J.M. et al. SARS-CoV-2, COVID-19 and the aging immune system. *Nature Aging* **1**, 769-782 (2021).
81. Lee, S. et al. Virus-induced senescence is a driver and therapeutic target in COVID-19. *Nature* **599**, 283-289 (2021).
82. Camell, C.D. et al. Senolytics reduce coronavirus-related mortality in old mice. *Science* **373** (2021).
83. Li, S. et al. Cellular metabolic basis of altered immunity in the lungs of patients with COVID-19. *Med Microbiol Immunol* **211**, 49-69 (2022).
84. D'Agnillo, F. et al. Lung epithelial and endothelial damage, loss of tissue repair, inhibition of fibrinolysis, and cellular senescence in fatal COVID-19. *Sci Transl Med* **13**, eabj7790 (2021).
85. Parimon, T. et al. Potential mechanisms for lung fibrosis associated with COVID-19 infection. *QJM* **116**, 487-492 (2023).
86. Evangelou, K. et al. Pulmonary infection by SARS-CoV-2 induces senescence accompanied by an inflammatory phenotype in severe COVID-19: possible implications for viral mutagenesis. *Eur Respir J* **60** (2022).
87. Chen, J., Wu, H., Yu, Y. & Tang, N. Pulmonary alveolar regeneration in adult COVID-19 patients. *Cell Res* **30**, 708-710 (2020).
88. Liao, M. et al. Single-cell landscape of bronchoalveolar immune cells in patients with COVID-19. *Nat Med* **26**, 842-844 (2020).
89. Merad, M. & Martin, J.C. Pathological inflammation in patients with COVID-19: a key role for monocytes and macrophages. *Nat Rev Immunol* **20**, 355-362 (2020).
90. Garcia-Nicolas, O., Godel, A., Zimmer, G. & Summerfield, A. Macrophage phagocytosis of SARS-CoV-2-infected cells mediates potent plasmacytoid dendritic cell activation. *Cell Mol Immunol* **20**, 835-849 (2023).
91. Burton, D. & Stolzing, A. Cellular senescence: Immunosurveillance and future immunotherapy. *Ageing Res Rev* **43**, 17-25 (2018).
92. Lo, J.A. & Fisher, D.E. The melanoma revolution: from UV carcinogenesis to a new era in therapeutics. *Science* **346**, 945-9 (2014).
93. Robert, C. et al. Nivolumab in previously untreated melanoma without BRAF mutation. *N Engl J Med* **372**, 320-30 (2015).
94. Hoenicke, L. & Zender, L. Immune surveillance of senescent cells--biological significance in cancer- and non-cancer pathologies. *Carcinogenesis* **33**, 1123-6 (2012).
95. Kang, T.W. et al. Senescence surveillance of pre-malignant hepatocytes limits liver cancer development. *Nature* **479**, 547-51 (2011).
96. Xue, W. et al. Senescence and tumour clearance is triggered by p53 restoration in murine liver carcinomas. *Nature* **445**, 656-60 (2007).
97. Ruscetti, M. et al. NK cell-mediated cytotoxicity contributes to tumor control by a cytostatic drug combination. *Science* **362**, 1416-1422 (2018).
98. Tirosh, I. et al. Dissecting the multicellular ecosystem of metastatic melanoma by single-cell RNA-seq. *Science* **352**, 189-96 (2016).

99. Teschendorff, A.E., Breeze, C.E., Zheng, S.C. & Beck, S. A comparison of reference-based algorithms for correcting cell-type heterogeneity in Epigenome-Wide Association Studies. *BMC Bioinformatics* **18**, 105 (2017).
100. Newman, A.M. et al. Robust enumeration of cell subsets from tissue expression profiles. *Nat Methods* **12**, 453-7 (2015).
101. Coppe, J.P. et al. Senescence-associated secretory phenotypes reveal cell-nonautonomous functions of oncogenic RAS and the p53 tumor suppressor. *PLoS Biol* **6**, 2853-68 (2008).
102. Acosta, J.C. et al. Chemokine signaling via the CXCR2 receptor reinforces senescence. *Cell* **133**, 1006-18 (2008).
103. Kuilman, T. et al. Oncogene-induced senescence relayed by an interleukin-dependent inflammatory network. *Cell* **133**, 1019-31 (2008).
104. Biran, A. et al. Senescent cells communicate via intercellular protein transfer. *Genes Dev* **29**, 791-802 (2015).
105. Jin, S. et al. Inference and analysis of cell-cell communication using CellChat. *Nat Commun* **12**, 1088 (2021).
106. Senturk, S. et al. Transforming growth factor-beta induces senescence in hepatocellular carcinoma cells and inhibits tumor growth. *Hepatology* **52**, 966-74 (2010).
107. Reimann, M. et al. Tumor stroma-derived TGF-beta limits myc-driven lymphomagenesis via Suv39h1-dependent senescence. *Cancer Cell* **17**, 262-72 (2010).
108. Buckley, S. et al. BMP4 signaling induces senescence and modulates the oncogenic phenotype of A549 lung adenocarcinoma cells. *Am J Physiol Lung Cell Mol Physiol* **286**, L81-6 (2004).
109. Zhu, D., Wu, J., Spee, C., Ryan, S.J. & Hinton, D.R. BMP4 mediates oxidative stress-induced retinal pigment epithelial cell senescence and is overexpressed in age-related macular degeneration. *J Biol Chem* **284**, 9529-39 (2009).
110. Korbecki, J. et al. in International Journal of Molecular Sciences (2020).
111. Price, M.A. et al. CSPG4, a potential therapeutic target, facilitates malignant progression of melanoma. *Pigment Cell Melanoma Res* **24**, 1148-57 (2011).
112. Gurrea-Rubio, M. & Fox, D.A. The dual role of CD6 as a therapeutic target in cancer and autoimmune disease. *Front Med (Lausanne)* **9**, 1026521 (2022).
113. Zhang, C. et al. STAT3 Activation-Induced Fatty Acid Oxidation in CD8(+) T Effector Cells Is Critical for Obesity-Promoted Breast Tumor Growth. *Cell Metab* **31**, 148-161.e5 (2020).
114. Malta, T.M. et al. Machine Learning Identifies Stemness Features Associated with Oncogenic Dedifferentiation. *Cell* **173**, 338-354.e15 (2018).
115. Gennady, K., Vladimir, S. & Alexey, S. Fast gene set enrichment analysis. *bioRxiv*, 060012 (2019).
116. Agarwal, S., Graepel, T., Herbrich, R., Har-Peled, S. & Roth, D. Generalization Bounds for the Area Under the ROC Curve. *Journal of Machine Learning Research* **6**, 393--425 (2005).
117. Teschendorff, A.E. & Enver, T. Single-cell entropy for accurate estimation of differentiation potency from a cell's transcriptome. *Nat Commun* **8**, 15599 (2017).
118. Yeung, K.Y., Fraley, C., Murua, A., Raftery, A.E. & Ruzzo, W.L. Model-based clustering and data transformations for gene expression data. *Bioinformatics* **17**, 977-87 (2001).
119. Fang, Z., Liu, X. & Peltz, G. GSEApy: a comprehensive package for performing gene set enrichment analysis in Python. *Bioinformatics* **39** (2023).
120. Wang, W. et al. Independent component analysis based gene co-expression network inference (ICAnet) to decipher functional modules for better single-cell clustering and batch integration. *Nucleic Acids Res* **49**, e54 (2021).

121. Haghverdi, L., Buettner, F. & Theis, F.J. Diffusion maps for high-dimensional single-cell analysis of differentiation data. *Bioinformatics* **31**, 2989-98 (2015).
122. Subramanian, A. et al. Gene set enrichment analysis: a knowledge-based approach for interpreting genome-wide expression profiles. *Proc Natl Acad Sci U S A* **102**, 15545-50 (2005).
123. Colaprico, A. et al. TCGAbiolinks: an R/Bioconductor package for integrative analysis of TCGA data. *Nucleic Acids Res* **44**, e71 (2016).
124. Calcinotto, A. et al. Cellular Senescence: Aging, Cancer, and Injury. *Physiol Rev* **99**, 1047-1078 (2019).
125. Gorgoulis, V. et al. Cellular Senescence: Defining a Path Forward. *Cell* **179**, 813-827 (2019).
126. Nighat, N., Zhenqing, Y., Yidong, C., Xiaojing, W. & Siyuan, Z. Benchmarking supervised signature-scoring methods for single-cell RNA sequencing data in cancer. *bioRxiv*, 2021.06.29.450404 (2021).
127. Zhang, Y., Alexander, P.B. & Wang, X.F. TGF-beta Family Signaling in the Control of Cell Proliferation and Survival. *Cold Spring Harb Perspect Biol* **9** (2017).

Supplementary Files

This is a list of supplementary files associated with this preprint. Click to download.

- SupplementaryTables.xlsx
- Extendeddatafigures.pdf
- SupplementaryTables.xlsx
- Extendeddatafigures.pdf